Letter

# Computing Riemann zeros with light scattering

Sunkyu Yu [1,*] Xianji Piao [2,†] and Namkyoo Park [3,‡]

[1] *Intelligent Wave Systems Laboratory, Department of Electrical and Computer Engineering, Seoul National University, Seoul 08826, Korea*
[2] *Wave Engineering Laboratory, School of Electrical and Computer Engineering, University of Seoul, Seoul 02504, Korea*
[3] *Photonic Systems Laboratory, Department of Electrical and Computer Engineering, Seoul National University, Seoul 08826, Korea*

(Received 2 September 2024; revised 21 November 2024; accepted 26 November 2024; published 23 December 2024)

Finding hidden order within disorder is a common interest in material science, wave physics, and mathematics. The Riemann hypothesis, stating the locations of nontrivial zeros of the Riemann zeta function, tentatively characterizes statistical order in the seemingly random distribution of prime numbers. This famous conjecture has inspired various connections with different branches of physics, recently with non-Hermitian physics, quantum field theory, trapped-ion qubits, and hyperuniformity. Here we develop the computing platform for the Riemann zeta function by employing classical scattering of light. We show that the Riemann hypothesis suggests the landscape of semi-infinite optical scatterers for the perfect reflectionless condition under the Born approximation. To examine the validity of the scattering-based computation, we investigate the asymptotic behaviors of suppressed reflections with the increasing number of scatterers and the emergence of multiple scattering. The result provides another bridge between classical physics and the Riemann zeros, exhibiting the design of wave devices inspired by number theory.

DOI: 10.1103/PhysRevB.110.L220201

Mathematics allows for linking seemingly unrelated phenomena in different domains of physics. The Riemann hypothesis [1] is a representative example, bridging classical, quantum, and relativistic physics through number theory [2]. For the Riemann zeta function $\zeta(s) = \sum_{n=1}^{\infty} \frac{1}{n^s}$ with a complex variable $s = \sigma + it$, where $\sigma$ and $t$ are real, this cornerstone conjecture claims that the locations of the nontrivial zeros for $t \neq 0$ are restricted to $\sigma = 1/2$. The most important result of understanding the locations of the nontrivial Riemann zeros would be the quantification of prime number distribution due to its relationship with the prime counting function, which forms the basis for number theory [3,4]. Efforts to connect the conjecture to physics have unveiled $\zeta(s)$ in chaotic resonators [2], parity-time-symmetric Hamiltonians [5,6], relativistic scattering [7], and trapped-ion qubits [8]. The Hilbert-Pólya conjecture [9] also suggests that the nontrivial Riemann zeros correspond to real eigenvalues of a Hermitian operator.

Material science is another branch exploring the Riemann hypothesis. Due to the similarity between material classification and number theory in discovering hidden order, the intermediate regime between order and uncorrelated disorder has attracted substantial attention in exploring the hypothesis. For example, there has been an attempt to understand the locations of the Riemann zeros using quasicrystals [10,11]. The distribution of prime numbers has also been examined through the concept of hyperuniformity [12–14], which reveals the suppression of long-range fluctuations in the pattern of prime numbers [15,16]. Very recently, the correspondence between the quasitransparent states, in terms of the Landauer resistance of the logarithmic chain, and the Riemann zeros has been investigated [17] inspired by the log-time sampling [18].

Here, we revisit classical scattering theory to develop light-based computing of the Riemann zeta function through engineered scatterers. We propose the $\sigma$-Riemann scatterer composed of the logarithmically spaced one-dimensional (1D) semi-infinite scatterers with $\sigma$-power-law-decayed scattering amplitudes. We demonstrate that the Riemann hypothesis corresponds to the complete reflectionless condition only at the (1/2)-Riemann scatterer under the Born approximation, where the locations of the Riemann zeros denote the zero-reflection wavelength of light. We estimate the valid range of highly suppressed reflection at the Riemann-zero wavelengths, by examining a finite number of scatterers and multiple scattering beyond the Born approximation. The result offers insights into the non-Hermitian generalization of the Hilbert-Pólya conjecture and the design of reflectionless optical structures using the hyperuniformity with reciprocal-space shifts.

*Riemann zeta functions in light scattering*. To investigate the relationship between light scattering and the Riemann zeta function, we review 1D multiple-scattering theory [19]. Consider a wave equation $d^2\psi/dx^2 + [V_0 + V(x)]\psi = 0$, where $\psi$ is a wave function, and $V_0$ and $V(x)$ are a constant and a spatially varying potential, respectively. The potentials in

*Contact author: sunkyu.yu@snu.ac.kr
†Contact author: piao@uos.ac.kr
‡Contact author: nkpark@snu.ac.kr

*Published by the American Physical Society under the terms of the Creative Commons Attribution 4.0 International license. Further distribution of this work must maintain attribution to the author(s) and the published article's title, journal citation, and DOI.*

our example correspond to the landscape of permittivity in nonmagnetic optical media [20,21].

Motivated by the semi-infinite summation of $\zeta(s) = \sum_{n=1}^{\infty} \frac{1}{n^s}$, we consider a material that is asymptotically homogeneous as $x$ approaches negative infinity: $V(x \to -\infty) = 0$. Scattering from the material is examined with the plane-wave incidence from $x \to -\infty$, $\psi_{\rm I} = \psi_0 \exp(ik_0 x)$, which is the solution of the Helmholtz equation $d^2\psi/dx^2 + V_0\psi = 0$, where $V_0 = k_0^2$ and $k_0 = 2\pi/\lambda \geqslant 0$ for the wavelength $\lambda$. With the scattering wave function $\psi_{\rm S}$, the total wave function $\psi$ is determined by the 1D Lippmann-Schwinger equation [19], as $\psi = \psi_{\rm I} + \psi_{\rm S} = \psi_{\rm I} + \frac{1}{4\pi}\int_{-\infty}^{+\infty} V(x')\psi(x')G(x,x')dx'$, where $G(x, x') = (2\pi i/k_0)\exp(ik_0|x-x'|)$ is the 1D Green's function satisfying $d^2G(x, x')/dx^2 + V_0G(x, x') = -4\pi\delta(x-x')$ for the Dirac delta function $\delta(x)$. By defining the scattering operator $M$ as

$$(M\varphi)(x) = \frac{i}{2k_0}\int_{-\infty}^{+\infty} V(x')\varphi(x')e^{ik_0|x-x'|}dx', \tag{1}$$

for an arbitrary wave function $\varphi(x)$, $\psi$ can be expressed as the Born series [19], $\psi = \psi_{\rm I} + \sum_{m=1}^{\infty}\psi_{S,m}$, where $\psi_{{\rm S},m} \triangleq M^m\psi_{\rm I}$ is the $m$th-order scattering wave function.

From this 1D scattering theory, we derive $\zeta(s)$ by tailoring $V(x)$. The inhomogeneous potential is implemented with an array of $N$ point scatterers, as $V(x) = V_N(x) \triangleq \sum_{n=1}^{N} d_n\delta(x-x_n)$, where $d_n$ and $x_n$ are the scattering amplitude and position of the $n$th scatterer, respectively, $N$ is the number of scatterers, and $x_n \leqslant x_{n+1}$ for all $n$. Among various forms of $\zeta(s)$, we focus on the form from the Dirichlet eta function [22,23]:

$$\zeta(s) = \frac{1}{1-2^{1-s}}\sum_{n=1}^{\infty}\frac{(-1)^{n+1}}{n^s}, \tag{2}$$

to guarantee convergence in the critical strip $\{s \in \mathbb{C} : 0 < {\rm Re}[s] = \sigma < 1\}$, which was proved to possess all the nontrivial zeros [4]. To derive Eq. (2), we define the $\sigma$-Riemann scatterer [Fig. 1(a)]—an array of $N$ scatterers having the logarithmically spaced distribution $x_n = x_0\log(n)$ and the alternating $\sigma$-power-law scattering amplitudes $d_n = (-1)^{n+1}d_0n^{-\sigma}$, as

$$V(x) = d_0\sum_{n=1}^{N}\frac{(-1)^{n+1}}{n^{\sigma}}\delta(x - x_0\log(n)), \tag{3}$$

where $x_0$ and $d_0$ are real- and complex-valued coefficients, respectively. The first-order scattering field between the $p$th and $(p+1)$th scatterers is obtained as follows (Note S1 in the Supplemental Material [24]):

$$\psi_{{\rm S},1}(x; x_p \leqslant x < x_{p+1}) = \frac{id_0\psi_0}{2k_0}\left[\left(\sum_{n=1}^{p}\frac{(-1)^{n+1}}{n^{\sigma}}\right)e^{+ik_0x} + \left(\sum_{n=p+1}^{N}\frac{(-1)^{n+1}}{n^{\sigma-2ik_0x_0}}\right)e^{-ik_0x}\right]. \tag{4}$$

The comparison between $\psi_{{\rm S},1}$ and $\psi_{\rm S}$ is shown in Fig. 1(b) (Note S2 in [24] for multiple scattering). The form of Eq. (3) is identical to the logarithmic chain for suppressed Landauer resistance in the recent study [17]. On the other hand, our approach, which starts from the first principle, enables not only the examination of internal fields from Eq. (4) but also the analytical extension to multiple-scattering analysis with the scattering operator $M$ as discussed later.

Equation (4) provides insight into the connection between the first-order scattering and the Riemann zeta function, leading to the following transmitted ($p \to \infty$) and reflected ($p = 0$) waves from the semi-infinite ($N \to \infty$) $\sigma$-Riemann scatterer:

$$\begin{aligned}\psi_{\rm T}(x; x \to \infty) &= \tfrac{id_0\psi_0e^{+ik_0x}}{2k_0}(1-2^{1-\sigma})\zeta(\sigma),\\ \psi_{\rm R}(x; x < x_1) &= \tfrac{id_0\psi_0e^{-ik_0x}}{2k_0}(1-2^{1-\sigma+2ik_0x_0})\zeta(\sigma-2ik_0x_0).\end{aligned} \tag{5}$$

Equation (5) demonstrates that both the transmitted and the reflected waves from the semi-infinite $\sigma$-Riemann scatterer are proportional to the Riemann zeta function $\zeta(s)$ under the first-order Born approximation. When considering a practical measurement setup and the exploration of nontrivial Riemann zeros with $s \in \mathbb{C}$, the measurement of the reflected wave is suitable for light-based computation of the Riemann zeta function. Notably, ${\rm Im}[s] = -2k_0x_0$ can be controlled by the optical wavelength $\lambda = 2\pi/k_0$. Figures 1(c) and 1(d) describe the $\lambda$-dependent amplitude and phase of the Riemann zeta function $\zeta(\sigma - 4\pi ix_0/\lambda)$, respectively, within the critical strip $0 < \sigma < 1$, exhibiting the Riemann-zero wavelengths ("×" symbols).

*Optically computed Riemann zeros.* Using the design of the Riemann scatterer, we revisit the Riemann hypothesis, which states that the nontrivial zeros of $\zeta(s)$ exist only at ${\rm Re}[s] = \sigma = 1/2$. Because $\zeta(s^*) = [\zeta(s)]^*$, it is well known [4] that the nontrivial zeros $s^0 = 1/2 + it^0$ lead to the other zeros $s^0 = 1/2 - it^0$, which can be directly compared with $s = \sigma - 4\pi ix_0/\lambda$ in $\psi_{\rm R}(x) \sim \zeta(s)$. Therefore, the Riemann hypothesis claims that the complete suppression of the first-order scattering from the $\sigma$-Riemann scatterer can be achieved only with the (1/2)-Riemann scatterer, which requires the scattering amplitudes $d_n = (-1)^{n+1}d_0n^{-1/2}$ ($\sigma$ row in Table I). The location of the nontrivial Riemann zeros $t^0$ determines the perfect reflectionless wavelength $\lambda^0 = 4\pi x_0/t^0$ ($t$ row in Table I). The conjugate relation $\zeta(s^*) = [\zeta(s)]^*$ corresponds to electromagnetic reciprocity in light scattering, achieving the reflectionless condition for the incidence with the opposite-directional wave vector $-2\pi/\lambda^0$ ($s^*$ row in Table I). We emphasize that higher-order scatterings $\psi_{{\rm S},m}(x) = M^{m-1}\psi_{{\rm S},1}(x) = 0$ ($m = 2, 3, \ldots, \infty$) are not completely suppressed because the complete suppression of $\psi_{{\rm S},1}(x)$ occurs only in $x < 0$.

The Riemann scatterer presents a unique approach to the Hilbert-Pólya conjecture [9] and its generalization into non-Hermitian physics [5,6]. Consider the decomposition of the Hermitian Hamiltonian $H$ for the (1/2)-Riemann scatterer into two subsystem Hamiltonians, which separate the forward ($H_{\rm F}$)

TABLE I. Correspondence between the Riemann hypothesis and the first-order scattering.

| | Riemann hypothesis | First-order scattering from the $\sigma$-Riemann scatterer |
|---|---|---|
| Re[$s$] | $\sigma = 1/2$ | Scattering amplitudes |
| | for $\zeta(s) = 0$ | $\lvert d_n\rvert = d_0/n^{1/2}$ for $\psi_R(x) = 0$ |
| Im[$s$] | $t = t^0$ | Incident wavelength |
| | for $\zeta(s) = 0$ | $\lambda^0 = 4\pi x_0/t^0$ for $\psi_R(x) = 0$ |
| $s^*$ | $\zeta(s^{0*}) = 0$ | Wave-vector reciprocity |
| | when $\zeta(s^0) = 0$ | $(\pm 2\pi/\lambda^0)$ for $\psi_R(x) = 0$ |

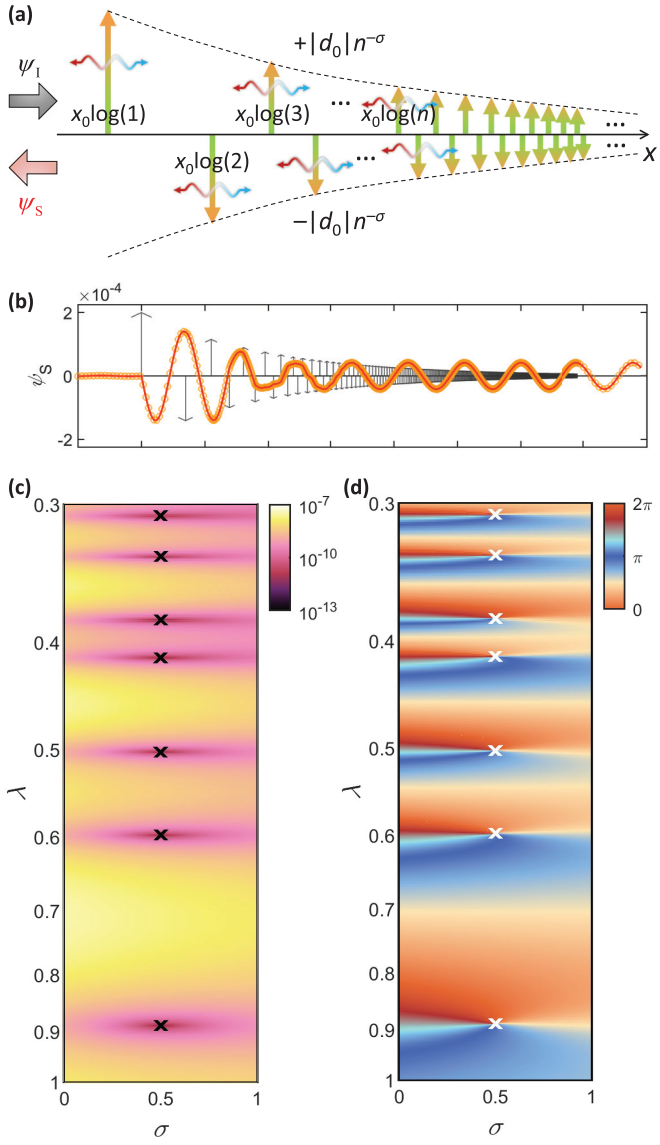



FIG. 1. Riemann scatterer. (a) The $\sigma$-Riemann scatterer: a semi-infinite array of logarithmically spaced scatterers with a $\sigma$-power-law distribution of sign-alternating scattering amplitudes. (b) An example of scattering from the (1/2)-Riemann scatterer for $d_0 = 0.001$. The arrows illustrate point scatterers. Red solid lines denote $\psi_S$ calculated by the scattering matrix method [25] (Note S2 in [24]). Orange circles denote $\psi_{S,1}$ obtained from Eq. (4). $N = 1000$, $x_0 = 1$, and $\psi_0 = 1$. (c), (d) The Riemann zeta function $\zeta(\sigma - 4\pi i x_0/\lambda)$ in the critical strip: amplitude (c) and phase (d). The symbols "×" denote the first seven nontrivial zeros.

and backward ($H_B$) paths in the region where $x < 0$. Due to scattering, $H_F$ and $H_B$ are generally coupled, and therefore, each Hamiltonian itself is non-Hermitian with complex eigenvalues. However, under the first-order Born approximation, $H_F$ (and $H_B$) can exhibit real eigenvalues without the coupling to $H_B$ (and to $H_F$) at the reflectionless wavelengths $\lambda^0$. Therefore, $H_F$ could serve as the non-Hermitian Hamiltonian for the generalized Hilbert-Pólya conjecture. The Riemann hypothesis states that such decomposition is possible only with the potential landscape of the (1/2)-Riemann scatterer.

The Riemann scatterer also exhibits an intriguing connection to the concept of hyperuniformity [12–14,26,27], allowing for interpreting the (1/2)-Riemann scatterer as correlated disorder. For a 1D inhomogeneous material composed of point particles, $V(x) = V_N(x) \stackrel{\Delta}{=} \sum_{n=1}^{N} d_n \delta(x - x_n)$, the structure factor $S(k)$ is given by $S(k) = |\sum_{n=1}^{N} d_n \exp(-ikx_n)|^2$. Hyperuniformity is defined by the asymptotic behavior of the structure factor, $S(k \to 0) \to 0$, in the thermodynamic limit, which corresponds to the suppression of infinite-wavelength density fluctuations [12,14,26]. For the Riemann scatterer, the above definition of the structure factor leads to $S(k) = d_0^2 |\sum_{n=1}^{N} (-1)^{n+1} n^{-(\sigma + ikx_0)}|^2$, which approaches $S(k) = d_0^2 |\zeta(\sigma + ikx_0)|^2$ at $N \to \infty$ in the critical strip. Therefore, each nontrivial Riemann zero in the Riemann scatterer corresponds to the complete halt of the density fluctuation at $\lambda^0 = 4\pi x_0/t^0$, which can be considered the reciprocal-space translation of the perfect hyperuniformity from $k = 0$ to $2k_0$.

*Riemann scatterer as evolving scattering networks.* Although the correspondence between the Riemann zeta function and the $\sigma$-Riemann scatterer is achieved with a semi-infinite ($N \to \infty$) array of weak ($d_0 \to 0$) and point-particle [$\delta(x - x_0 \log(n))$] scatterers, its measurable implementation requires breaking such ideal constraints. First, we investigate the effect of $N$ on the reflectance by multiple scattering, $R = |\psi_S(x < 0)|^2/|\psi_0|^2$, which is an experimentally measurable quantity. Figure 2(a) shows the reflectance map $R(N,\lambda)$ under the weak scattering condition ($d_0 = 0.001$), which exhibits converging behaviors with increasing $N$. We note that the increase in $N$ can be considered the evolutionary change of a material [27]. Such an evolving model reveals a unique nature of nontrivial Riemann zeros: nonoscillatory suppression of the reflectance. Figure 2(b) illustrates the evolutions of the reflectance $R$ for different wavelengths near the second nontrivial Riemann-zero wavelength $\lambda^{0,2}$. The result shows that the reflectance decreases monotonically with increasing $N$ at the wavelength of a nontrivial Riemann zero, which is

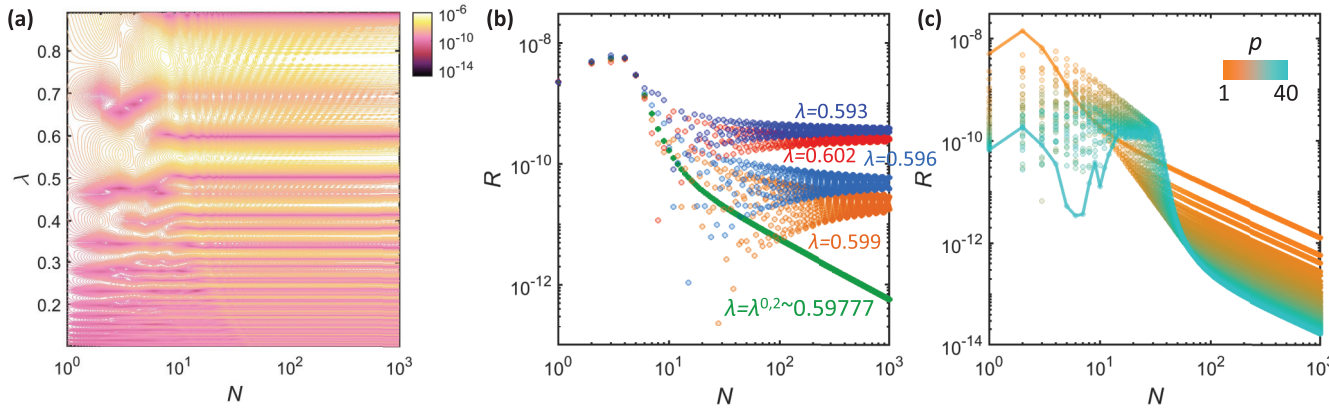



FIG. 2. Evolution of the (1/2)-Riemann scatterer. (a) The multiple-scattering reflectance $R$ as a function of the particle number $N$ and the wavelength $\lambda$. (b) The evolutions of $R$ with respect to $N$ at the second nontrivial Riemann-zero wavelength $\lambda^{0,2} \sim 0.597\,77$ and its neighboring wavelengths ($\lambda = 0.593$, 0.596, 0.599, and 0.602). (c) The evolutions of $R$ with respect to $N$ at the nontrivial Riemann-zero wavelengths $\lambda^{0,p}$ ($p = 1, 2, \ldots, 40$). The solid lines highlight the cases of $p = 1$ and 40. $x_0 = 1$, $d_0 = 0.001$, and $\psi_0 = 1$.

confirmed with the evolution of $R$ at other nontrivial zeros [Fig. 2(c) for $\lambda^{0,p}$ with $p = 1, 2, \ldots, 40$)]. In contrast, the evolution of $R$ oscillates with $N$ at other wavelengths. In terms of the evolving scattering network model [27], the monotonic decrease of $R$ corresponds to the optimal suppression of the density fluctuation at a given $k$ of $S(k)$. Similar to the design of stealthy hyperuniformity using the evolving network [27], the (1/2)-Riemann scatterer provides the optimal suppression of the density fluctuation at $k$ defined by the nontrivial Riemann zeros.

*Beyond the Born approximation*. Another restriction is the Born approximation. It is well known that the convergence of the Born series is valid when the spectral radius of the operator $M$ is less than unity [28]. This condition is determined by $d_0$, $N$, and the size of each scatterer [19]. While preserving the point-particle scatterer configuration, Fig. 3 illustrates the effect of $d_0$ and $N$. We note that the linear response between $\log(d_0)$ and $\log(R)$ guarantees the validity of the first-order Born approximation, which enables the light-based computing of nontrivial Riemann zeros. The increase of $d_0$ and $N$ breaks this approximation, while the breakdown occurs more rapidly at the lower-$p$ zero with a larger $\lambda$. It is because an array of scatterers seems to be more clustered for the incidence of a larger $\lambda$, which breaks the constraint on the scatterer size despite the point shape of each scatterer.

Extending the discussion on multiple scattering, we lift another restriction for practical implementation—the point-particle condition. We replace each point particle of the $\sigma$-Riemann scatterer [Fig. 4(a)] with the corresponding layer of finite thickness [Fig. 4(b)], where the center of the layer is $x_n = x_0 \log(n)$. The array of these layers is embedded in a homogeneous material $V_0 = k_0^2$. To reproduce the scattering from the ideal $\sigma$-Riemann scatterer, the thickness and potential of the $n$th layer are set to be $l_n = l_0 n^{-\sigma}$ and $V_n = [1 + (-1)^{n+1}\rho]^2 V_0$, respectively, where $l_0$ is the thickness of the first layer and $\rho$ is the coefficient of material inhomogeneity for two-phase multilayers [Fig. 4(b)]. The designed layer corresponds to the effective realization of the point particle $d_n \delta(x - x_n)$, where $d_0 \sim (2k_0^2\rho) l_0$ for $d_n = (-1)^{n+1} d_0 n^{-\sigma}$ under weak scattering assumption (Note S3 in [24]).

Figure 4(c) shows the multiple-scattering reflectance from the multilayered Riemann scatterer with increasing $N$ at the wavelengths of nontrivial Riemann zeros ($p = 1$, 5,

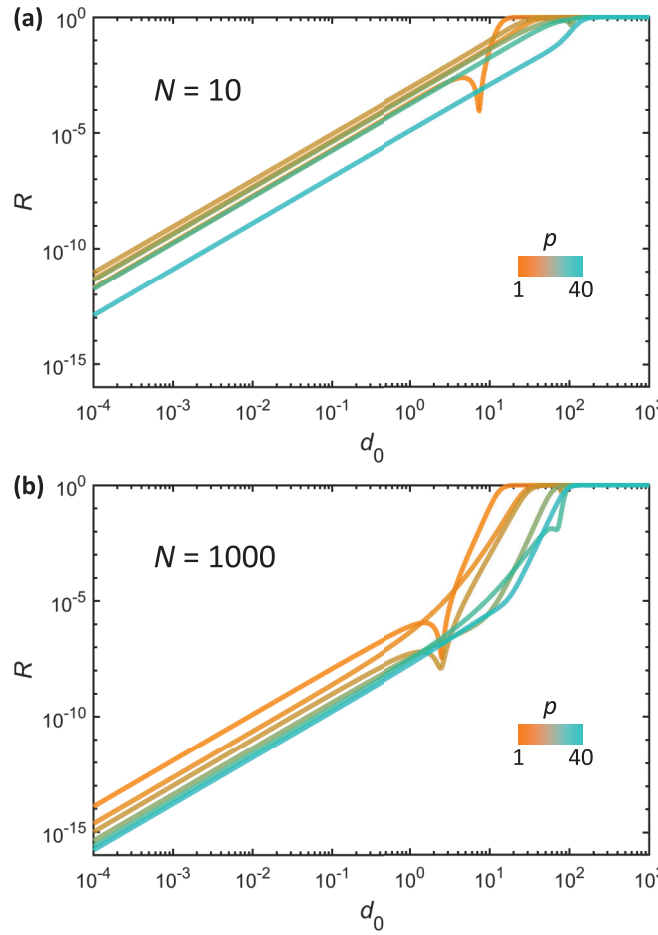



FIG. 3. Beyond the Born approximation. (a), (b) The multiple-scattering reflectance $R$ as a function of $d_0$ at the wavelengths of nontrivial zeros $\lambda^{0,p}$ ($p = 1, 2, \ldots, 40$): $N = 10$ (a) and $N = 1000$ (b). All the other parameters are the same as those in Fig. 2.

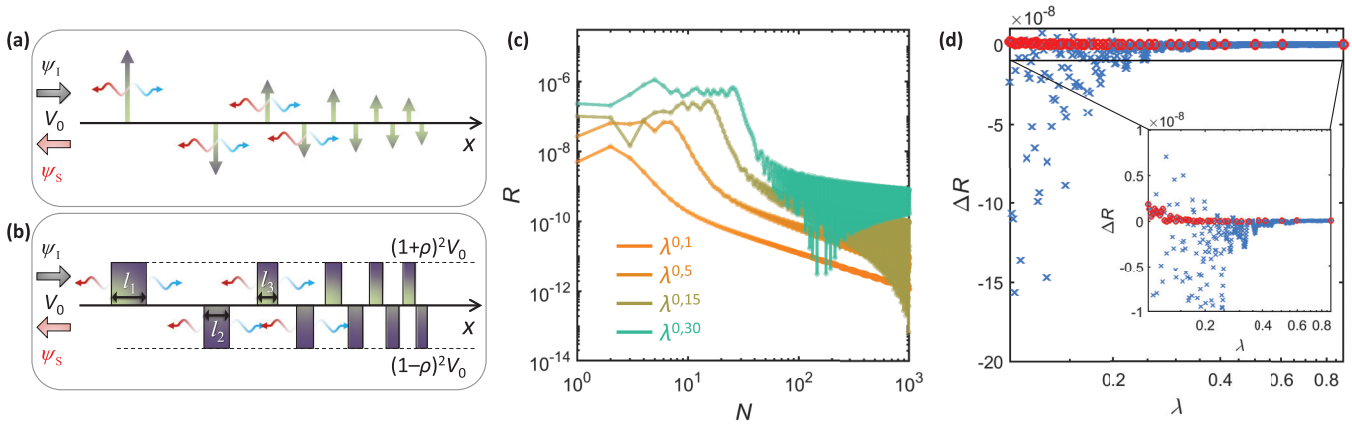



FIG. 4. Multilayered Riemann scatterer. (a), (b) Reproduction of the point-particle Riemann scatterer (a) with the multilayered one (b). (c) The evolution of reflectance with respect to $N$ for the Riemann-zero wavelengths of $\lambda^{0,1}$, $\lambda^{0,5}$, $\lambda^{0,15}$, and $\lambda^{0,30}$. (d) The difference between the multiple-scattering reflection and the first-order reflection, $\Delta R = R - |\psi_R|^2$, as a function of the wavelength $\lambda$. The red circles highlight the Riemann-zero wavelengths. The inset emphasizes a narrower range of $\Delta R$ for better visibility. The thickness coefficient and material inhomogeneity are set to be $l_0 = 0.01$ and $\rho = 10^{-3}$, respectively. All the other parameters are the same as those in Fig. 2.

15, and 30). Due to the broken Born approximation with $d_0 \sim (2k_0^2\,\rho)l_0$, the suppression of reflectance is weakened at shorter wavelengths, which correspond to higher-$p$ Riemann zeros. However, the relative suppression of reflectance at the Riemann-zero wavelengths compared to their nearby wavelengths significantly increases at higher $p$, as shown in the exemplified comparison among $p = 2$, 15, and 30 in Note S4 of [24]. This observation is confirmed with the wavelength dependency of the discrepancy $\Delta R = R - |\psi_R|^2$ in Fig. 4(d), which quantifies the contribution from higher-order scattering to the reflectance. As shown, the magnitude of $\Delta R$ maintains a relatively very low value at each Riemann-zero wavelength (red circles) when compared with the values of its nearby wavelengths. This result demonstrates that the ratio of higher-order scattering originating from the broken Born approximation is sufficiently small at the Riemann zeros, enabling the identification of the Riemann zeros even at higher $p$.

The correspondence between the first-order scattering and the Riemann zeta function belongs to the class of wave-based mathematical operations, such as diffractive optical computing [29], filtering [30], interferometric matrix multiplications [31], metamaterial equation solvers [32], and classical spin-model optimization [33]. The relationship $\exp(2ik_0x_n) = n^{2ik_0x_0}$ for $x_n = x_0\log(n)$ demonstrates that logarithmically spaced scatterers pave the way to the wave-based computing of other special functions: the prime zeta function $P(s) = \sum_{p\in\text{primes}} \frac{1}{p^s}$, the Hurwitz zeta function $\zeta(s,a) = \sum_{n=0}^{\infty} \frac{1}{(n+a)^s}$, the reciprocal of the Riemann zeta function, and the Möbius function $\mu(n)$.

In the realm of disordered photonics, the Riemann scatterer extends hyperuniformity with reciprocal-space shifts forms a class of logarithmically spaced correlated disorder toward reflectionless design. Especially, the semi-infinite form of the Riemann scatterer introduces a unique mechanism for scattering suppression, distinct from antireflection coating, reflectionless potential profiles [34,35], and reflectionless scattering modes [36], all of which primarily focus on finite-size scatterers. A comparable case would be parity-time-symmetric crystals for unidirectional transport [37], because nonuniform scattering amplitudes $d_n$ can be replaced with complex-valued wave numbers $k_0$. The complete suppression of reflection in the (1/2)-Riemann scatterer with logarithmically spaced scatterers also offers insights into the design of log-periodic antennas with directional radiation [38].

In conclusion, we developed the concept of the Riemann scatterer, which results in the scattering quantified by the Riemann zeta function. The Riemann hypothesis claims that completely zero reflection from the scatterer can be achieved only with a (1/2)-power-law distribution of scattering amplitudes. We examined the valid range of our theory by numerically investigating multiple-scattering cases under the broken Born approximation. This approach allows for experimentally accessible design using two-phase scatterers in contrast to the recent study on electric resistance [17]. For example, the relation $d_0 \sim (2k_0^2\rho)l_0$ and the valid range for the Born approximation, $d_0 < 1$ in Fig. 3(b), lead to the design of layer thicknesses $l_n$ and the target index contrast $\rho$. Further research is highly desirable to develop subsystem Hilbert-Pólya Hamiltonians for the Riemann scatterer, design other special functions, link to well-known formulas in this field [39,40], and extend the theory to multiple-scattering regimes, thereby bridging physics and number theory.

*Acknowledgments*. We acknowledge financial support from the National Research Foundation of Korea (NRF) through the Basic Research Laboratory (Grant No. RS-2024-00397664), Young Researcher Program (Grant No. 2021R1C1C1005031), and Midcareer Researcher Program (Grant No. RS-2023-00274348), all funded by the Korean Government. This work was supported by Creative-Pioneering Researchers Program and the BK21 FOUR program of the Education and Research Program for Future ICT Pioneers in 2024, through Seoul National University. We also acknowledge administrative support from SOFT Foundry Institute.

[1] B. Riemann, Ueber die anzahl der primzahlen unter einer gegebenen grosse, Ges. Math. Werke **2**, 2 (1859).

[2] D. Schumayer and D. A. Hutchinson, *Colloquium*: Physics of the Riemann hypothesis, Rev. Mod. Phys. **83**, 307 (2011).

[3] L. J. Goldstein, A history of the prime number theorem, Am. Math. Mon. **80**, 599 (1973).

[4] H. M. Edwards, *Riemann's Zeta Function* (Courier Corporation, North Chelmsford, MA, 2001), Vol. 58.

[5] C. M. Bender, D. C. Brody, and M. P. Müller, Hamiltonian for the zeros of the Riemann zeta function, Phys. Rev. Lett. **118**, 130201 (2017).

[6] G. Sierra and J. Rodríguez-Laguna, $H = xp$ model revisited and the Riemann zeros, Phys. Rev. Lett. **106**, 200201 (2011).

[7] G. N. Remmen, Amplitudes and the Riemann zeta function, Phys. Rev. Lett. **127**, 241602 (2021).

[8] R. He, M.-Z. Ai, J.-M. Cui, Y.-F. Huang, Y.-J. Han, C.-F. Li, G.-C. Guo, G. Sierra, and C. E. Creffield, Riemann zeros from Floquet engineering a trapped-ion qubit, npj Quantum Inf. **7**, 109 (2021).

[9] J. Derbyshire, *Prime Obsession: Bernhard Riemann and the Greatest Unsolved Problem in Mathematics* (Joseph Henry Press, Washington, D.C., 2003).

[10] F. Dyson, Birds and frogs, Notices Amer. Math. Soc. **56**, 212 (2009).

[11] L. Dal Negro, *Optics of Aperiodic Structures: Fundamentals and Device Applications* (CRC, Boca Raton, FL, 2013).

[12] S. Torquato and F. H. Stillinger, Local density fluctuations, hyperuniformity, and order metrics, Phys. Rev. E **68**, 041113 (2003).

[13] S. Torquato, Hyperuniformity and its generalizations, Phys. Rev. E **94**, 022122 (2016).

[14] S. Torquato, Hyperuniform states of matter, Phys. Rep. **745**, 1 (2018).

[15] S. Torquato, G. Zhang, and M. de Courcy-Ireland, Uncovering multiscale order in the prime numbers via scattering, J. Stat. Mech. (2018) 093401.

[16] S. Torquato, G. Zhang, and M. De Courcy-Ireland, Hidden multiscale order in the primes, J. Phys. A: Math. Theor. **52**, 135002 (2019).

[17] D. S. Citrin, Quasitransparent states in the logarithmic chain and nontrivial zeros of the Riemann zeta function, Phys. Rev. B **110**, L081406 (2024).

[18] H. Olkkonen and J. T. Olkkonen, Log-time sampling of signals: Zeta transform, Open J. Discr. Math. **1**, 62 (2011).

[19] A. Gonis and W. H. Butler, *Multiple Scattering in Solids* (Springer Science & Business Media, New York, 1999).

[20] J. D. Jackson, *Classical Electrodynamics* (Wiley, New York, 1999).

[21] S. Longhi, Quantum-optical analogies using photonic structures, Laser Photonics Rev. **3**, 243 (2009).

[22] Y. D. Sergeyev, On accuracy of mathematical languages used to deal with the Riemann zeta function and the Dirichlet eta function, P-Aic Numbers Ultra. Anal., Appl. **3**, 129 (2011).

[23] M. S. Milgram, Integral and series representations of Riemann's zeta function and Dirichlet's eta function and a medley of related results, J. Math. **2013**, 181724 (2013).

[24] See Supplemental Material at http://link.aps.org/supplemental/10.1103/PhysRevB.110.L220201 for derivation of the first-order scattering (Note S1), multiple scattering from the point-particle Riemann scatterer (Note S2), multiple scattering from the multilayered Riemann scatterer (Note S3), and suppressed Riemann-zero reflection in multilayered Riemann scatterers (Note S4), which includes Ref. [25].

[25] S. G. Tikhodeev, A. L. Yablonskii, E. A. Muljarov, N. A. Gippius, and T. Ishihara, Quasiguided modes and optical properties of photonic crystal slabs, Phys. Rev. B **66**, 045102 (2002).

[26] S. Yu, C.-W. Qiu, Y. Chong, S. Torquato, and N. Park, Engineered disorder in photonics, Nat. Rev. Mater. **6**, 226 (2021).

[27] S. Yu, Evolving scattering networks for engineering disorder, Nat. Comput. Sci. **3**, 128 (2023).

[28] G. Osnabrugge, S. Leedumrongwatthanakun, and I. M. Vellekoop, A convergent Born series for solving the inhomogeneous Helmholtz equation in arbitrarily large media, J. Comput. Phys. **322**, 113 (2016).

[29] J. Hu, D. Mengu, D. C. Tzarouchis, B. Edwards, N. Engheta, and A. Ozcan, Diffractive optical computing in free space, Nat. Commun. **15**, 1525 (2024).

[30] S. Shukurov and C. Valagiannopoulos, Ultra-sharp angular filtering of far-field signals with graded-index multilayers, IEEE Trans. Antennas Propag. **71**, 6995 (2023).

[31] H. Zhou, J. Dong, J. Cheng, W. Dong, C. Huang, Y. Shen, Q. Zhang, M. Gu, C. Qian, and H. Chen, Photonic matrix multiplication lights up photonic accelerator and beyond, Light Sci. Appl. **11**, 30 (2022).

[32] N. Mohammadi Estakhri, B. Edwards, and N. Engheta, Inverse-designed metastructures that solve equations, Science **363**, 1333 (2019).

[33] N. G. Berloff, M. Silva, K. Kalinin, A. Askitopoulos, J. D. Töpfer, P. Cilibrizzi, W. Langbein, and P. G. Lagoudakis, Realizing the classical *XY* Hamiltonian in polariton simulators, Nat. Mater. **16**, 1120 (2017).

[34] J. Lekner, Reflectionless eigenstates of the $\mathrm{sech}^2$ potential, Am. J. Phys. **75**, 1151 (2007).

[35] S. Yu, X. Piao, and N. Park, Bohmian photonics for independent control of the phase and amplitude of waves, Phys. Rev. Lett. **120**, 193902 (2018).

[36] A. D. Stone, W. R. Sweeney, C. W. Hsu, K. Wisal, and Z. Wang, Reflectionless excitation of arbitrary photonic structures: A general theory, Nanophotonics **10**, 343 (2020).

[37] Z. Lin, H. Ramezani, T. Eichelkraut, T. Kottos, H. Cao, and D. N. Christodoulides, Unidirectional invisibility induced by $\mathcal{PT}$-symmetric periodic structures, Phys. Rev. Lett. **106**, 213901 (2011).

[38] R. Carrel, The design of log-periodic dipole antennas, *1958 IRE International Convention Record* (IEEE, New York, 1966), p. 61.

[39] T. S. Trudgian, An improved upper bound for the argument of the Riemann zeta-function on the critical line II, J. Number Theory **134**, 280 (2014).

[40] A. Odlyzko, Zeros of the Riemann zeta function: Conjectures and computations, in *Foundations of Computational Mathematics Conference*, Minnesota, 2002.